Energy and Buildings 75 (2014) 321–329

Contents lists available at ScienceDirect

Energy and Buildings

journal homepage: www.elsevier.com/locate/enbuild

Distributed lighting control with daylight and occupancy adaptation

Niels van de Meugheuvel[a,b], Ashish Pandharipande[a,*], David Caicedo[a], P.P.J. van den Hof[b]

[a] Philips Research, High Tech Campus, 5656 AE Eindhoven, The Netherlands
[b] Eindhoven University of Technology, The Netherlands

ARTICLE INFO

Article history:
Received 29 August 2013
Received in revised form 13 January 2014
Accepted 6 February 2014

Keywords:
Distributed lighting control
PI controllers
Daylight and occupancy adaptation

ABSTRACT

A distributed lighting system of multiple intelligent luminaires is considered for providing daylight and occupancy adaptive illumination. Each intelligent luminaire has a light sensor and an occupancy sensor that provides information on local light level and presence, respectively, and has a controller that adapts dimming level of the light source and a communication module. The illumination objective is to provide a desired average illuminance value over occupied/unoccupied zones at the workspace, specified in turn by occupancy-based set-points at corresponding light sensors. Two classes of proportional-integral (PI) controllers are considered to adapt the dimming levels of the luminaires to varying daylight levels under two networking scenarios. In one scenario, each controller operates stand-alone, sharing no information across other controllers, and has information about global occupancy. In the second scenario, controllers exchange control information within a neighborhood. The performance of the considered controllers is evaluated using photometric data from a DIALux implementation of an example open-plan office under different daylight and occupancy scenarios.

1. Introduction

Lighting is a major portion of the electrical energy consumption in commercial buildings [1]. The energy consumption in lighting systems may be reduced by suitable design of lighting control systems. Energy savings in lighting control systems may be realized by adapting to two dynamic aspects in the environment – varying amount of daylight and changes in occupancy. Various studies [2–5] have shown that considerable energy savings may be realized by such adaptation in cellular and open-office environments using simulated office models and in experimental office settings. While energy reduction is an important aspect, paying attention to the visual comfort needs of occupant users in terms of illuminance requirements is also important. In this paper, the design and evaluation of daylight and occupancy adaptive controllers for a distributed intelligent luminaire system is considered under two networking scenarios.

The lighting system under consideration consists of multiple intelligent luminaires. Each luminaire has a light sensor and an occupancy sensor. These sensors respectively measure the total illuminance level and determine binary occupancy within their fields of view. The output of the sensors is input to the associated controller that adapts the dimming level and controls the artificial light output of that luminaire. Each luminaire also has a communication module. We consider two networking scenarios. In the first scenario, stand-alone controllers are considered wherein there is no communication across luminaires. In the second scenario, the controllers may communicate with a set of neighboring controllers.

The dimming levels of each luminaire are to be determined by corresponding controllers such that the total artificial light output contribution, in combination with daylight contribution, results in net illuminance above desired levels at the workspace plane. Denote W_o and W_u to be the respective average illuminance values desired in an occupied and unoccupied zone at the workspace; a zone being a logical partitioning, for instance that defines work desks, of the physical horizontal workspace plane. European norms for office lighting for instance recommend minimum average illuminance values of $W_o = 500$ lx and $W_u = 300$ lx [6]. The illuminance targets at the workspace plane are specified in terms of sensor set-points at corresponding light sensors. These set-points are determined in a night-time calibration step. In the absence of daylight, the luminaires are dimmed to a level so that the desired illuminance, say W_o, is achieved and the corresponding light sensor measurements $\{r_{o,m}\}$ then are stored as the associated set-points. Let $r_{o,m}$ and $r_{u,m}$ be respectively the set-points of the mth light sensor corresponding to occupancy and non-occupancy. Then the control objective is to at least achieve this set-point, while limiting overshoot and oscillations in dimming (i.e. system should

* Corresponding author. Tel.: +31 40 2749741.
E-mail addresses: ashish.p@philips.com, pashish@ieee.org (A. Pandharipande).

http://dx.doi.org/10.1016/j.enbuild.2014.02.016
0378-7788/

achieve steady-state), and achieving power savings. Overshoot is the peak value compared to the final steady-state. We set the overshoot at the workspace plane to a maximum of 20%. This limits in turn the visual annoyance that a user might experience over the period that a controller seeks to achieve its reference. The study in [7], for instance, reports that positive changes up to 141 lx did not cause occupant annoyance at an illuminance target of 500 lx.

In this paper, we consider two classes of PI controllers. One is the classical PI controller that seeks to achieve the light sensor set-point. The other is a PI controller with offset, which seeks to achieve a positively biased set-point. We consider PI controllers with offset motivated by the observations regarding daylight in [8,9], where a single light sensor-driven lamp system was considered. The authors in [8,9] observed that a controller that seeks to achieve a constant set-point may result in lower illuminance at the workspace plane as the amount of daylight entering the space increases. This happens since the ratio of daylight contribution at the workspace plane to the contribution at the light sensor is not the same as that of artificial light and moreover changes over the day. In this paper, we evaluate the two PI controllers in a networked lighting control system setting.

A centralized lighting control system was considered in [10] for occupancy adaptive lighting and a simplex algorithm was used to solve the resulting optimization problem, with the system extended in [4] to take into account spatio-temporal daylight variations. Both formulations assumed knowledge of light distribution at the workspace plane. Distributed optimization algorithms for lighting control with daylight and occupancy adaptation were proposed in [3,11], under networking and information exchange constraints. Under different system settings, and wherein users carried light sensors, linear programming and sequential quadratic programming approaches were proposed for centralized lighting control [12,13]. A wireless networked lighting system with light sensors at work desks was considered in [14]. In [15], a distributed lighting system was proposed with light sensors at desks, and equipped with a controller, which control luminaires in a neighborhood using infra-red communication. Desk-placed light sensor measurements can be quite sensitive to environmental changes such as occupant movements, thus affecting illumination performance of the lighting system. We will hence focus on ceiling-mounted sensor configurations that are employed in practice [3,9].

The remainder of the paper is organized as follows. In Section 2, we present an analytical model of the lighting control system. The PI controllers in stand-alone mode are described and analyzed in Section 3, and the distributed system is analyzed using a multiple-input, multiple-output (MIMO) system model in Section 4. The performance of these controllers is evaluated using an example open-plan office model implemented in DIALux, and results are discussed in Section 5. The design of PI controllers with communication is presented in Section 6 and performance evaluation results are shown in Section 7. Conclusions are drawn in Section 8.

Notation: A matrix with element $A_{i,j}$ denoting the element in the ith row, jth column is written as A. The transpose and inverse, if exists, are respectively written as A^T and A^{-1}. An $M \times 1$ vector with ith element b_i is written as $\mathbf{b} = [b_1(t), \ldots, b_M(t)]^T$. The matrix $\mathrm{diag}([\alpha_1, \ldots, \alpha_M]^T)$ is an $M \times M$ diagonal matrix with the diagonal element in the ith row, ith column being α_i. Vectors with all elements 0 and 1 respectively are denoted by $\mathbf{0}$ and $\mathbf{1}$. The first-order derivative of a signal $u(t)$ is written as $\dot{u}(t)$. The sets of natural numbers and real numbers are respectively denoted as $\mathbb{N}$ and $\mathbb{R}$.

2. System model

Consider a lighting system with M ceiling-based intelligent luminaires. Let the luminaire be dimmed using pulse width modulation (PWM). Let the nth luminaire be dimmed linearly with duty cycle $u_n(t)$ at time t, where $0 \le u_n(t) \le 1$. The illumination value at the mth light sensor, in lux, at time t can be expressed as [3]

$$y_m(t) = \sum_{n=1}^{M} G_{m,n} u_n(t) + d_m(t), \quad m = 1, \ldots, M. \tag{1}$$

Here $G_{m,n}$ is the illumination value at the mth light sensor when the nth luminaire is dimmed at its maximum, while all other luminaires are off and there is no other source of light, $d_m(t)$ is the illumination contribution at the mth light sensor in lux due to daylight at time t.

Let the workspace plane be divided into N logical zones. The illumination value at zone j may be written as

$$w_j(t) = \sum_{n=1}^{M} H_{j,n} u_n(t) + p_j(t), \quad j = 1, \ldots, N, \tag{2}$$

where $p_j(t)$ is the average illumination in lux contributed at the jth zone due to daylight at time t, $H_{j,n}$ is the average illumination of the jth zone in lux when the nth luminaire is dimmed at its maximum, all other luminaires are off and there is no other source of light. In matrix form, the model is written as

$$\mathbf{y}(t) = G\mathbf{u}(t) + \mathbf{d}(t) \tag{3a}$$

$$\mathbf{w}(t) = H\mathbf{u}(t) + \mathbf{p}(t), \tag{3b}$$

where

$$\begin{aligned}
\mathbf{y}(t) &= [y_1(t), \ldots, y_M(t)]^T, \\
\mathbf{u}(t) &= [u_1(t), \ldots, u_M(t)]^T, \\
G &= \begin{bmatrix} G_{1,1} & G_{1,2} & \ldots & G_{1,M} \\ G_{2,1} & G_{2,2} & \ldots & G_{2,M} \\ \vdots & \vdots & \ddots & \vdots \\ G_{M,1} & G_{M,2} & \ldots & G_{M,M} \end{bmatrix}, \\
\mathbf{d}(t) &= [d_1(t), \ldots, d_M(t)]^T, \\
\mathbf{w}(t) &= [w_1(t), \ldots, w_N(t)]^T, \\
H &= \begin{bmatrix} H_{1,1} & H_{1,2} & \ldots & H_{1,M} \\ H_{2,1} & H_{2,2} & \ldots & H_{2,M} \\ \vdots & \vdots & \ddots & \vdots \\ H_{N,1} & H_{N,2} & \ldots & H_{N,M} \end{bmatrix}, \\
\mathbf{p}(t) &= [p_1(t), \ldots, p_N(t)]^T.
\end{aligned}$$

3. Stand-alone illumination controller

We first consider a stand-alone controller, wherein controller m seeks to determine the dimming level u_m so as to at least achieve the light sensor reference set-point $r_{o,m}$, if occupancy sensor m determines occupancy, or set-point $r_{u,m}$, if occupancy sensor m determines non-occupancy but there is global presence. This is the simplest networking scenario with no interaction with other controllers sought.

The stand-alone controller is depicted in Fig. 1. Each controller samples with sample rate T_s. The sampling of the controllers is not synchronous, reflecting the distributed nature of the lighting control system.

Following (1), the illuminance at the mth light sensor can be written as

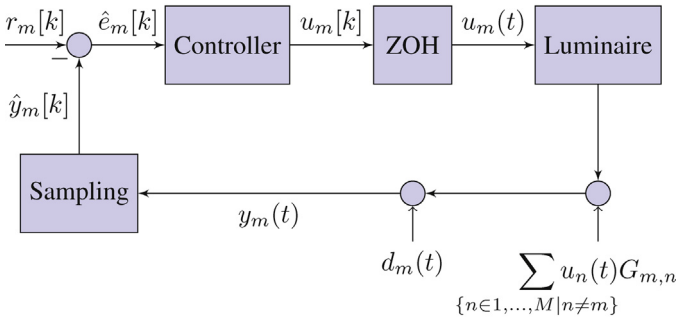

Fig. 1. Block diagram of a stand-alone controller.

$$\hat{y}_m(kT_s+\tau_m) = G_{m,m}u_m((k-1)T_s+\tau_m+\tau_c) + d_m(kT_s+\tau_m) + \sum_{\{n\in 1,\dots,M|n\neq m\}} G_{m,n}u_n(kT_s+\tau_m), \quad (4)$$

where $0 \le \tau_m \le T_s$ is a uniformly distributed random delay which is constant for each controller, $k \in \mathbb{N}$ and τ_c is the delay between sampling and updating the zero-order-hold (ZOH) filter. The last term in (4) represents the influence of other luminaires on the mth luminaire. Because the mth luminaire also influences other luminaires, this effect is referred to as coupling. Note that if the coupling is zero, the overall lighting control system is equivalent to M stand-alone controllers. The input to the controller is

$$\hat{e}_m(k) = r_m(k) - \hat{y}_m(k). \quad (5)$$

During a night time calibration step, the mth controller obtains $G_{m,m}$ and the references $r_{u,m}$ and $r_{o,m}$.

3.1. Generalized controller

Two types of controllers are studied. One, the classical PI controller, that seeks to achieve the reference. Two, a PI controller with offset that seeks to achieve a point that is positively biased with respect to the reference. Both controllers can be described in the following general form:

$$u_m(k) = \alpha_m u_m(k-1) + \beta_m \hat{e}_m(k) + \zeta_m, \quad (6)$$

where α_m, β_m and ζ_m are constants in $\mathbb{R}$.

The state space representation of the generalized controller (6) is

$$\begin{aligned} x_m(k+1) &= \alpha_m x_m(k) + \beta_m \hat{e}_m(k) + \zeta_m \\ u_m(k) &= \alpha_m x_m(k) + \beta_m \hat{e}_m(k) + \zeta_m, \end{aligned} \quad (7)$$

where $x_m(k)$ represents the state, which is equal to $u_m(k-1)$.

3.1.1. Saturation

In (6), the physical limits of the luminaire dimming levels were not accounted for. The duty cycle for each luminaire is limited between 0 and 1, i.e. $0 \le u_m(k) \le 1$. To make sure that the controller output is within these bounds, a saturation function is applied to the controller output. The saturation function is defined b y

$$\text{sat}(x_m) = \begin{cases} 1, & \text{if } x_m > 1 \\ x_m, & \text{if } 0 \le x_m \le 1 \\ 0, & \text{if } x_m < 0. \end{cases} \quad (8)$$

The saturated output of the controller is stored in memory and used to calculate the next output, so the state space representation with saturation of the generalized controller is

$$\begin{aligned} x_m(k+1) &= \text{sat}\left(\alpha_m x_m(k) + \beta_m \hat{e}_m(k)\right) \\ u_m(k) &= \text{sat}\left(\alpha_m x_m(k) + \beta_m \hat{e}_m(k)\right). \end{aligned} \quad (9)$$

The next two sections analyze the two PI controllers, ignoring the effect of saturation for simplicity of analysis.

3.2. Classical PI controller

Under the assumption that the daylight changes slowly compared to the sample rate of the controller and neglecting the coupling term, the estimate $\tilde{y}_m(k+1)$ of $\hat{y}_m(k+1)$ is given by

$$\tilde{y}_m(k+1) = u_m(k)G_{m,m} + d_m(k+1). \quad (10)$$

For brevity of notation, $(kT_s+\tau_m)$ is written as (k) and τ_c has been neglected for simplicity. The controller needs to follow $r_m(k)$, so when reaching the reference, we must have

$$\begin{aligned} r_m(k) &= \tilde{y}_m(k+1) \\ &= u_m(k)G_{m,m} + d_m(k+1). \end{aligned} \quad (11)$$

From (11), $u_m(k)$ can be calculated so as to keep $\tilde{y}_m(k+1)$ close to $r_m(k)$,

$$u_m(k) = \frac{r_m(k) - d_m(k+1)}{G_{m,m}}. \quad (12)$$

Because daylight changes slowly, $d(k+1) \approx d(k)$, so

$$u_m(k) \approx \frac{r_m(k) - d_m(k)}{G_{m,m}}. \quad (13)$$

The daylight term $d_m(k)$ can be extracted from (11) as

$$d_m(k) = \tilde{y}_m(k) - u_m(k-1)G_{m,m}. \quad (14)$$

Substituting (14) into (13), the expression for the controller is obtained as

$$u_m(k) = \frac{\hat{e}_m(k)}{G_{m,m}} + u_m(k-1). \quad (15)$$

Eq. (15) is a classical PI controller [16], which can be written in the form (6), where

$$\begin{aligned} \alpha_m &= 1, \\ \beta_m &= G_{m,m}^{-1}, \\ \zeta_m &= 0. \end{aligned} \quad (16)$$

With constant daylight and without coupling, this controller will achieve the reference in one step.

3.3. PI controller with offset

This class of PI controllers seeks to achieve a steady-state point that is positively biased with respect to the reference set-point. A specific class of such controllers was considered in [9] for a lighting system controlled by a single light sensor with all light sources driven to the same dimming level. In [8,9], it was observed that as the amount of daylight into a room increases, a controller that is designed to achieve the reference set-point results in lower illuminance value at the workspace plane than desired, under certain daylight scenarios. To address this, a daytime calibration step was introduced and a term with the ratio of daylight contribution at the workspace plane to the contribution at the light sensor was used in the controller design.

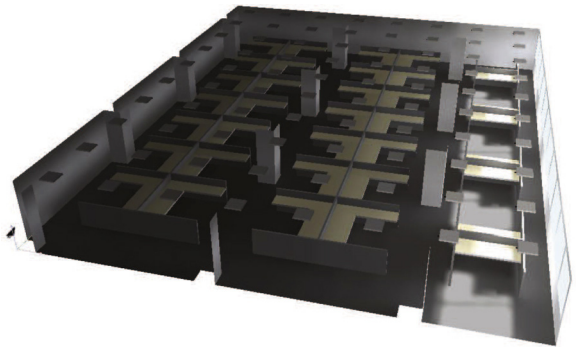

Fig. 2. Open-plan office with only daylight at 8:30 h; daylight is entering through windows on the right side of the room.

In Laplace domain, the controller in [8] may be written as

$$u(s) = \frac{\rho}{1+s\tau}e(s) + 1, \tag{17}$$

where $u(s)$ and $e(s)$ are the Laplace transforms of respectively $u(t)$ and $e(t) = r(t) - y(t)$, τ is a time constant and the parameter ρ is calibrated such that the illumination at the workspace plane equals the required illumination, for a given daylight distribution.

In the time domain, (17) may be written as

$$\dot{u}(t) = \frac{\rho e(t) - u(t) + 1}{\tau}. \tag{18}$$

Using the forward Euler method, we have in discrete form

$$\frac{u(k) - u(k-1)}{T_s} = \frac{\rho e(k) - u(k) + 1}{\tau}, \tag{19}$$

$$u(k) = \frac{\tau u(k-1) + \rho T_s \hat{e}(k) + T_s}{\tau + T_s}. \tag{20}$$

The controller can be expressed in the generalized form (6), with

$$\begin{aligned} \alpha_m &= \frac{\tau}{\tau + T_s}, \\ \beta_m &= \frac{\rho T_s}{\tau + T_s}, \\ \zeta_m &= \frac{1}{\tau + T_s}. \end{aligned} \tag{21}$$

3.4. Stability of the controller

If the coupling between the controllers and the saturation is ignored, the closed loop transfer from the reference input of the system to the output of the system can be described in the discrete Laplace domain as

$$\frac{Y_m(z)}{R_m(z)} = \frac{G_{m,m}\beta_m}{z - \alpha_m + G_{m,m}\beta_m}. \tag{22}$$

The system has one pole at

$$z_p = \alpha_m - G_{m,m}\beta_m. \tag{23}$$

For stability

$$|z_p| < 1 \tag{24}$$

should hold.

For the classical PI controller, using (16) we have $z_p = 0$. For the PI controller with offset, the pole equals

$$z_p = \frac{\tau - G_{m,m}\rho T_s}{\tau + T_s}. \tag{25}$$

When the stability requirement (24) is applied to (25), we obtain

$$-\frac{1}{G_{m,m}} < \rho < \frac{2\tau}{G_{m,m}T_s} + \frac{1}{G_{m,m}}. \tag{26}$$

4. MIMO system model

To evaluate the stability and steady-state behavior of the previously described controllers, we consider a model for the whole system of M controllers. First the entities in G are sorted by execution order. The first row represents the transfer to the first sensor which is sampled in the system. The first column represents the luminaire that belongs to the same controller as the first sensor. Denote the sorted matrix by $\hat{G}$. Then

$$\begin{aligned} \hat{y}_m(k) = \hat{G}_{m,m}u_m(k-1) + \sum_{m+1}^{M}\hat{G}_{m,n}u_n(k-1) \\ + \sum_{n=1}^{m-1}\hat{G}_{m,n}u_n(k) + \hat{d}_m(k), \end{aligned} \tag{27}$$

which can be written in vector notation as

$$\hat{\mathbf{y}}(k) = (\hat{G}_d + \hat{G}_u)\mathbf{u}(k-1) + \hat{G}_l\mathbf{u}(k) + \hat{\mathbf{d}}(k), \tag{28}$$

where $\hat{G}_d$ is the diagonal part of $\hat{G}$, $\hat{G}_u$ the strictly upper triangular part of $\hat{G}$, and $\hat{G}_l$ the strictly lower triangular part of $\hat{G}$, thus

$$\hat{G} = \hat{G}_d + \hat{G}_l + \hat{G}_u. \tag{29}$$

4.1. The closed loop system

Consider the controller, with $\mathbf{u}(k)$ as output vector and $\hat{\mathbf{e}}$ as input vector, given by

$$\begin{aligned} \mathbf{x}(k+1) &= \Psi\left(A\mathbf{x}(k) + B\hat{\mathbf{e}}(k) + \boldsymbol{\zeta}\right) \\ \mathbf{u}(k) &= \Psi\left(A\mathbf{x}(k) + B\hat{\mathbf{e}}(k) + \boldsymbol{\zeta}\right), \end{aligned} \tag{30}$$

where

$$\begin{aligned} A &= \mathrm{diag}\left([\alpha_1, \ldots, \alpha_M]^T\right), \\ B &= \mathrm{diag}\left([\beta_1, \ldots, \beta_M]^T\right), \\ \mathbf{x}(k) &= [x_1(k), \ldots, x_M(k)]^T \end{aligned} \tag{31}$$

and Ψ is the vector saturation function defined as

$$\Psi(\mathbf{x}) = [\mathrm{sat}(x_1), \ldots, \mathrm{sat}(x_M)]^T. \tag{32}$$

In the closed loop system, the input to the controller is

$$\hat{\mathbf{e}}(k) = \mathbf{r}(k) - \hat{\mathbf{y}}(k). \tag{33}$$

Define $\check{\mathbf{y}}$ as

$$\check{\mathbf{y}}(k) = \hat{\mathbf{y}}(k) - \mathbf{d}(k), \tag{34}$$

then the input to the controller is

$$\begin{aligned} \hat{\mathbf{e}}(k) &= \mathbf{r}(k) - \mathbf{d}(k) - \check{\mathbf{y}}(k) \\ &= \mathbf{q}(k) - \check{\mathbf{y}}(k), \end{aligned} \tag{35}$$

where $\mathbf{q}(k)$ is the input of the closed loop system, which is

$$\mathbf{q}(k) = \mathbf{r}(k) - \mathbf{d}(k). \tag{36}$$

Both the controller and the system are non-strictly proper, there is a direct connection from the input to the output.

Let

$$\Delta = I + B\hat{G}_l, \tag{37}$$

then if Δ is non-singular, the interconnected system is well-posed and the interconnection between the plant and the controller is [17, p. 275]

$$\mathbf{u} = \Delta^{-1}\Gamma\mathbf{x} + \Delta^{-1}B\mathbf{q} + \Delta^{-1}\boldsymbol{\zeta}, \tag{38}$$

Table 1
Specifications of the simulated room.

Number of luminaires	80
Luminaire type	Philips BBS 560 [18]
Room size	24 m × 19 m × 2.6 m
Number of zones	36
Height of workplane	0.76 m
W_o	500 lx
W_u	300 lx

where

$$\Gamma = A - B(\hat{G}_d + \hat{G}_u). \tag{39}$$

The closed loop system is described as

$$\begin{aligned} \mathbf{x}^+ &= \Psi(\Gamma\mathbf{x} + B\mathbf{q} + \boldsymbol{\zeta} - B\hat{G}_l\Psi(\Delta^{-1}(\Gamma\mathbf{x} + B\mathbf{q} + \boldsymbol{\zeta}))) \\ \mathrm{y} &= (\hat{G}_d + \hat{G}_u)\mathbf{x} + \hat{G}_l\Psi(\Delta^{-1}(\Gamma\mathbf{x} + B\mathbf{q} + \boldsymbol{\zeta})), \end{aligned} \tag{40}$$

where $\mathbf{x}^+$ is short notation for $\mathbf{x}(k+1)$, with index (k) omitted for brevity of notation.

4.2. Stability

The stability of the closed loop system, where the sensors sample in a particular order and disregarding the saturation, can be determined from (40) by evaluating the eigenvalues of the matrix $(I - B\hat{G}_l\Delta^{-1})\Gamma$. Each eigenvalue of this matrix needs to be within the unit ball for the closed loop system to be stable.

If the closed loop system is stable and no controller output saturates, in steady-state we have

$$\mathbf{x}_s = \mathbf{x}(k+1) = \mathbf{x}(k), \tag{41}$$

where $\mathbf{x}_s$ is the steady-state. Then using (41) and (40), we have

$$\mathrm{x}_s = (I - \Gamma + B\hat{G}_l\Delta^{-1}\Gamma)^{-1}(I - B\hat{G}_l\Delta^{-1})(B\mathrm{q}_s + \boldsymbol{\zeta}), \tag{42}$$

where

$$\mathbf{q}_s = \mathbf{r}_s - \mathbf{d}_s. \tag{43}$$

Vectors $\mathbf{r}_s$ and $\mathbf{d}_s$ represent constant reference and constant daylight values at light sensors.

5. Simulation results

Simulations were used to evaluate the performance of the controllers. For the PI controller, step responses are executed to analyze whether the overshoot is below the required maximum. The steady-state response of the PI controller is evaluated to check whether the minimum illumination constraint is met when a zone is occupied.

5.1. Modeling of the office lighting control system

By creating a model of an open-plan office in DIALux [19], matrices G, H and datasets $\mathbf{d}(t)$ and $\mathbf{p}(t)$ are obtained. The spacing between the luminaires is chosen such that the average illumination of the workplane is 500 lx with a duty cycle for all luminaires of 0.85. A rendering of the office is depicted in Fig. 2. The specifications of the room and lighting system are listed in Table 1. The surface reflectances of the various office elements are as follows: top of desks 60%, floor 20%, walls 50%, and ceiling 80%. These values were chosen to be within the European recommended norms for office lighting [6]. The lighting plan is depicted in Fig. 3, where the 80 blue rectangles depict luminaire locations, indexed with blue numbers and the red circles indicate light sensor and occupancy sensor locations. In the office there are 36 zones, indexed in Fig. 3 with black numbers. Angle λ indicates the orientation of the room relative to the north. In the model, the opening angle of the occupancy sensors is 90°. When a zone is occupied, the occupancy sensors within field-of-view are triggered. Light sensors are emulated as done in [3], and with opening angle of 90°. Matrices G and H are obtained by turning the luminaires individually at maximum intensity level and then measuring the illumination at each light sensor and zone. The largest elements of G are on the diagonal, since the contribution from a luminaire to the co-located light sensor is larger than at any other sensor. Daylight is obtained by simulating three days from 7.30 h until 19.30 h. On all three days, a clear sky is simulated. The three days are chosen such that there is variation in daylight intensity and the angle of the incoming daylight. For all three days the solar elevation angle, the angle between the center of the sun disk and the horizon, is different; the maximum solar elevation angle for scenarios A, B and C is respectively 60°, 30° and 26°. Properties of the simulated days are listed in Table 2. Controllers are simulated with an interval of 1 s, so $T_s = 1$.

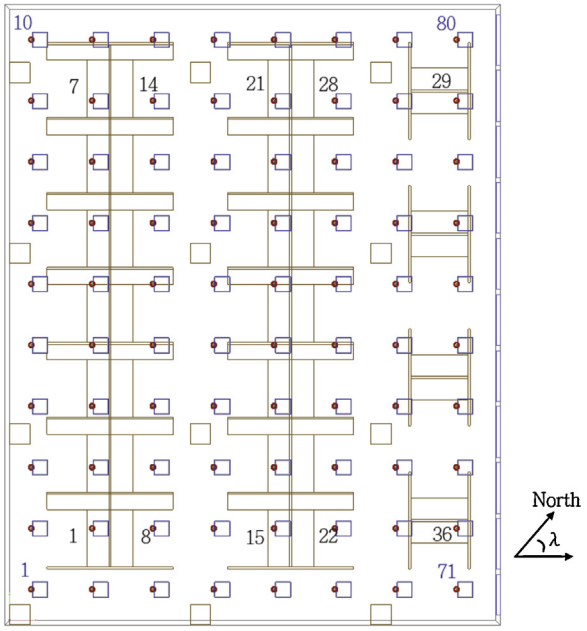

Fig. 3. Lighting plan with 80 luminaires (blue squares), with co-located light/occupancy sensors (red circles) and 36 zones. The windows are located on the right side. (For interpretation of the references to color in this figure legend, the reader is referred to the web version of this article.)

5.2. Simulation results

5.2.1. Occupancy dynamics

The scenario where a zone gets occupied while the surrounding zones are not occupied, is most prone to overshoot, because the influence on the step response of nearby luminaires is greatest in this situation. To test whether the overshoot is within limits, an occupancy step is simulated for each zone, for 200 different control sequence orderings, for each half an hour during simulation A, resulting in 187, 200 different step responses. The results are depicted in Fig. 4. The box plot shows the median as the red line, the 75th and 25th percentile values as the box boundaries, and points

Table 2
Daylight simulation properties.

Simulation	Date	λ	Max. solar elevation angle
A	15-07-12	110°	60°
B	15-10-12	130°	30°
C	15-02-12	130°	26°

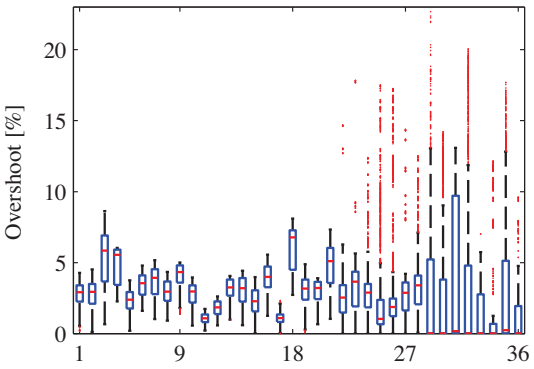

Fig. 4. Overshoot of illumination at each zone. Simulation *A* with classical PI controller.

outside the ±2.7 variance range are displayed individually by red dots. The maximum overshoot appears at zone 29 and is 22.7%. This is above the 20.0% limit, but only 0.006% of the simulations show a step response over the 20% limit. In 99% of the simulated cases, the overshoot is below 13.0%.

5.2.2. System start from zero-state

Fig. 5 shows the response of the system, when $\mathbf{x}(0) = \mathbf{0}$, $\mathbf{r} = \mathbf{r}_u$ and daylight was constant from simulation *B* at 17:30 h. In this scenario no states saturate, so this scenario is used to compare the simulation with the steady-state value from Eq. (42). The 2-norm of the difference of the states between (42) and the steady-state result of the simulation after 20 s is less than 10^{-10}, showing the numerical results match well with the analytical results.

5.2.3. PI with offset compared to PI

The PI controller with offset introduces an offset compared to the classical PI controller. Fig. 6 shows the average steady-state offset measured at the sensor for different values of ρ. For these results simulation *B* at 17:50 h. is used, where $\mathbf{r} = \mathbf{r}_u$. In this scenario no saturation occurs, so the result is not influenced by saturation and the steady-state value of $\hat{\mathbf{e}}(k)$, $\hat{\mathbf{e}}_s$ is zero in case the classical PI controller is used. The results in Fig. 6 show that the offset increases when ρ decreases. Note that a negative value for $\hat{e}_m$ results in a higher illumination of the zone close to the mth luminaire because of the negative feedback in the control loop.

Parameters α_m and β_m can not be the same for the PI with offset and the classical PI controllers. If for the PI controller with offset, $\rho = 0.05$ and $\tau = G_{m,m}\rho$, then the pole z_p for each SISO loop is at zero, which is also the case for the classical PI controller when $\beta_m = G_{m,m}^{-1}$.

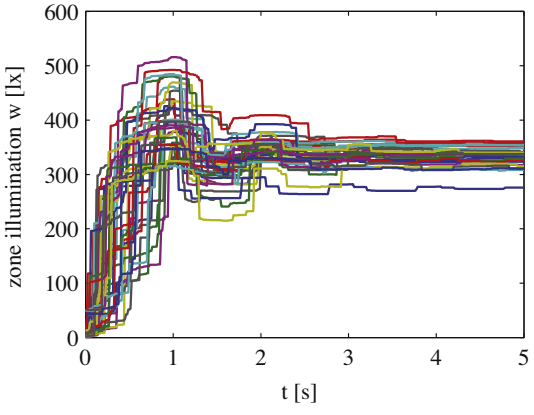

Fig. 5. Illumination of all zones with $\mathbf{x}(0) = \mathbf{0}$ for simulation *B* at 17:30 h. with classical PI controller.

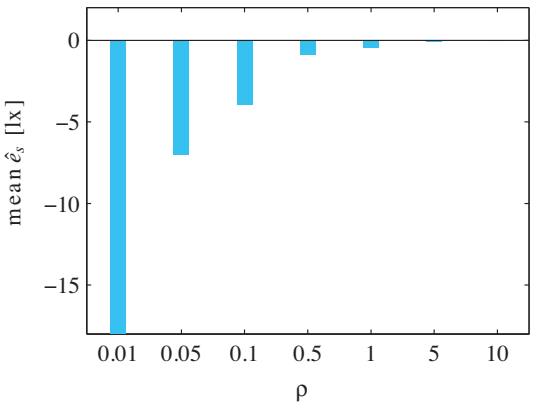

Fig. 6. Mean steady-state offset for different values of ρ with the PI with offset controller.

Fig. 7 shows the response of a step in the reference caused by occupancy detected at $t = 6$ for both the PI controller with offset and the classical PI controller with the aforementioned parameter values. Both step responses show similar transient behavior, due to the same pole location for both controllers, but the PI controller with offset shows an offset, resulting in greater workspace plane illumination.

5.2.4. Under-illumination

Light contribution from multiple luminaires is required to reach the minimum illuminance W_o. Under certain conditions, if one or several neighboring luminaires are dimmed low and do not contribute to the illuminance of a zone n, the illumination of the zone may not reach $w_{o,n}$. This is the case in simulation *B* at 8:30 h where zone 15 is occupied; Fig. 8 shows a daylight rendering in part of the office during this scenario. The sensors of the luminaires around luminaire 32 are illuminated by daylight and therefore contribute less to the illumination of zone 15, but the illumination of zone 15 by daylight is low. Therefore luminaire 32 is unable to reach the set reference. Figs. 9 and 10 show the steady-state output and duty cycles in this scenario. Luminaire 31 does not contribute to the illumination of zone 15 and therefore the steady-state illumination of zone 15 is only 412 lx, which is well below the target illumination W_o.

6. Networked control

Section 5.2.4 shows that scenarios exist where enough room to reach the minimum illumination level is available, but is

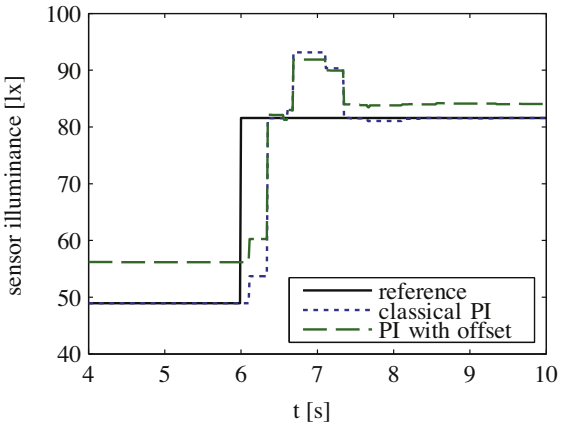

Fig. 7. Step responses of both PI with offset and PI controllers on luminaire 55.

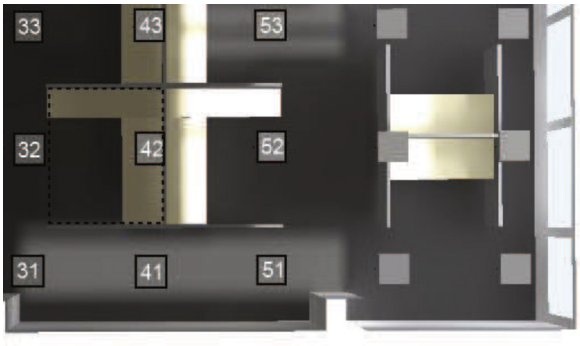

Fig. 8. Rendering of simulation *B* at 8:30 h. with the luminaires turned off. The dashed rectangle indicates the boundary of zone 15. The numbers are the indices of the luminaires.

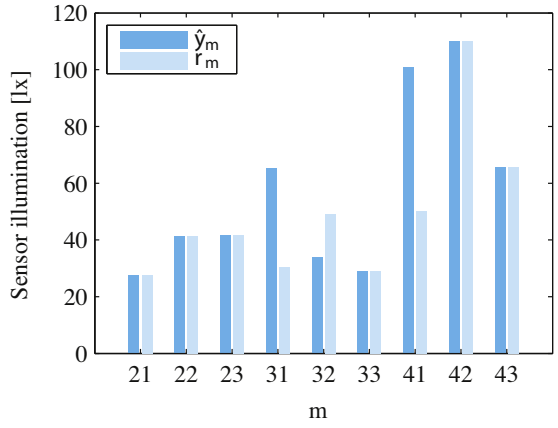

Fig. 9. Reference set-point and steady-state illuminance light sensor values in simulation *C*, where zone 15 is occupied.

not employed in the stand-alone control case, which results in under-illuminated zones. This issue can be resolved by adding communication to the classical PI controllers.

6.1. Networked controller

When the mth controller can not achieve reference $r_m(k)$, it will saturate at 1. When the duty cycles of neighboring controllers are less than 1, there is room available to achieve $r_m(k)$. Depending on the location of a luminaire, a controller may have 3, 5, or 8 neighbors, assuming a grid topology as depicted in Fig. 3. To exploit information from neighbors, a networked controller based on the classical PI controller is considered. The controller has the following state space description:

$$\begin{aligned} x_m^+ &= \text{sat}(\text{sat}(\alpha_m x_m + \beta_m e_m) + \max_i c_i \Phi_{i,m}) \\ u_m &= \text{sat}(\text{sat}(\alpha_m x_m + \beta_m e_m) + \max_i c_i \Phi_{i,m}) \\ c_m^+ &= \text{asat}((\alpha_m u_m + \beta_m e_m - u_m) G_{m,m} + c_m), \end{aligned} \tag{44}$$

where

$$\text{asat}(x_m) = \begin{cases} 0, & \text{if} \quad x_m \le 0 \\ x_m, & \text{otherwise.} \end{cases} \tag{45}$$

The $\text{asat}(x_m)$ function prevents the controller from sending messages with negative value. In (44), Φ is a constant matrix. If the mth luminaire communicates to the nth luminaire, then $\Phi_{m,n} > 0$, otherwise $\Phi_{m,n} = 0$. The value $\Phi_{m,n}$ is set at

$$\Phi_{m,n} = \frac{1}{G_m \cdot \mathbf{1} - G_{m,m}}, \tag{46}$$

where $G_m \cdot \mathbf{1}$ is the value of illumination at the mth sensor when all luminaires are set to 1.

The controller above may be interpreted in terms of the classical PI controller as follows.

- The mth classical PI controller calculates the output value according to (15). If this value is greater than one, one is subtracted and the remainder is sent to all controllers in the neighborhood. The message sent by the mth controller at the kth iteration is $c_m(k)$.
- If the mth controller receives a message from the ith controller, the message is multiplied with $\Phi_{i,m}$ and then added to the saturated output of the classical PI controller. The output is saturated before the received message is added, otherwise a negative value in the classical PI controller output might suppress the received message.
- If the mth controller receives multiple messages from different controllers, it will multiply all messages with the corresponding factor and add the largest value to the output of the classical PI controller.
- To ascertain that the contribution from neighbors to the mth controller by the message $c_m(k)$ is enough to make $\hat{e}_m = 0$, the message is integrated by the sender.

6.2. Saturation at step responses

Because the controller starts transmitting when it saturates at 1, existing overshoot is amplified for the networked controller. Therefore the β_m parameter needs to be tuned such that the controller does not saturate when it responds on a step in the reference. When $\beta_m = G_{m,m}^{-1}$, the PI controller tries to achieve the reference alone. In the lighting plan used, the mth luminaire is responsible for 30% to 50% of the illumination at the mth sensor. The rest of the illumination contribution at the light sensor comes from all other luminaires. To minimize the saturation at step responses, β_m is set at $(1/G_m \mathbf{1})$, where G_m is the mth row of G. Now the PI controller uses the total transfer to the mth sensor to calculate the output and will saturate less on step responses. The value of $G_m \mathbf{1}$ can be obtained during the night-time calibration step.

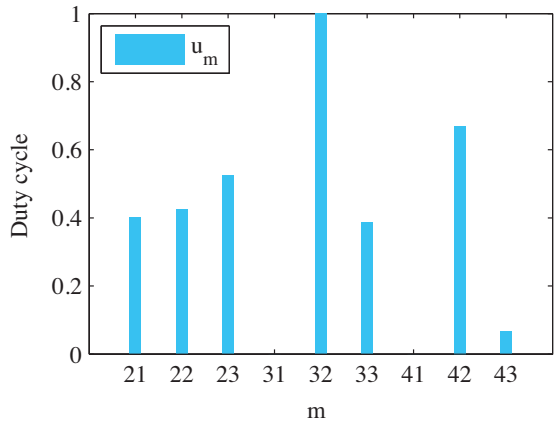

Fig. 10. Steady-state duty cycles of the luminaires in simulation *C*, where zone 15 is occupied.

7. Simulation results for networked control

7.1. Under-illumination

The scenario of Section 5.2.4 is simulated with the communicating controller. Fig. 11 shows the steady-state errors in the

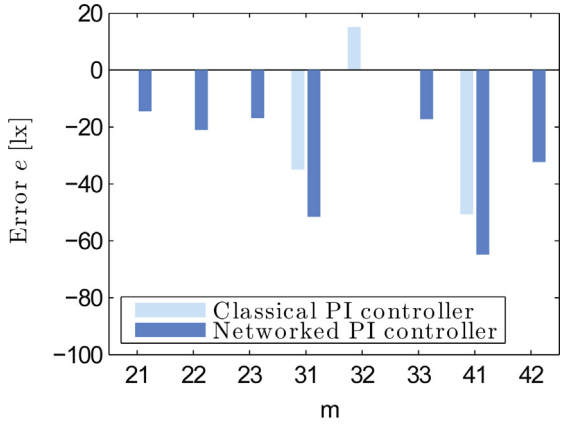

Fig. 11. Steady-state errors in scenario of under-illumination, with and without communication.

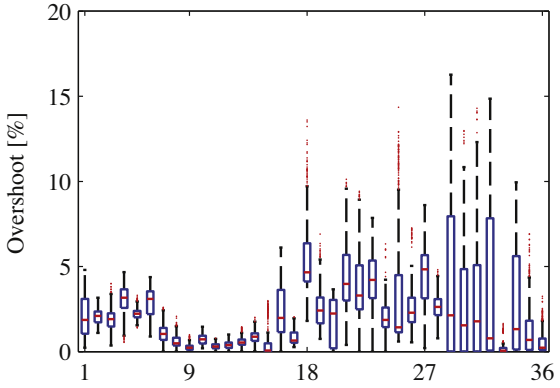

Fig. 13. Overshoot with the networked PI controller at each zone for 20 different sequence orders.

under-illumination scenario. The positive error on sensor 32 is resolved with communication. This results in more illumination of zone 15. With the PI controller, without communication, the illumination at zone 15 is only 412 lx. With the networked PI controller the illumination at zone 15 is 558 lx, so the zone is sufficiently illuminated. Fig. 12 shows the message sent by controller 32 in this scenario. When the zone is unoccupied at $t = 0$, a constant message is already sent because $r_{u,32}$ is not achieved. After zone 15 gets occupied at $t = 3$, the reference is set to $r_{o,32}$. More illumination by neighbors is required, c_{32} stabilizes at the point where $\hat{e}_{32} = 0$. At $t = 19$ the sensor detects that the zone is unoccupied and the reference is set to $r_{u,32}$ again.

7.2. Networked controller overshoot

Fig. 13 shows the same overshoot analysis as in Section 6.2. The median of the overshoot over all step responses is 1.54% and in 99% of the step responses, the overshoot is less than 11.0%. The overshoot requirement is thus met.

7.3. Illumination of the zones

To find out whether the minimum illumination constraint is met, 10 different static random occupancy scenarios where the probability that a zone is occupied is 0.3 are simulated for all daylight instants in Simulation *A*. For only one of the simulated scenarios, the minimum illumination constraint is not met. Fig. 14 shows the illumination for each zone and each simulated daylight realization. At zone 29, which is occupied, the illumination is 10% less than W_o between 17:30 h and 19:30 h. This is caused by the effect discussed in Section 3.3, where the ratio between the daylight on the sensor and daylight on the zone has changed, so the reference at the sensor is met, but the zone is under-illuminated.

7.4. Power consumption comparison

We compare the power consumption under the networked PI control lighting system with optimum centralized control lighting systems as well as one that uses the distributed optimization approach in [11]. Since the power consumption is directly proportional to the sum of duty cycles of the luminaires, we shall consider the average duty cycle in steady-state for comparison. The steady-state average duty cycle of controller (44) is compared to a centralized controller which solves the following linear programming problem:

$$\begin{aligned} \text{OPT1}: \min_{\mathbf{u}} \quad & \mathbf{u}\cdot\mathbf{1}^T \quad \text{s.t.} \\ & -G\,\mathbf{u} \le -\mathbf{q}_s \\ & \mathbf{0} \le \mathbf{u} \le \mathbf{1}, \end{aligned} \tag{47}$$

where the last inequality is element-wise. Only cases where $\hat{\mathbf{e}}_\mathbf{s} \le 0$ with the networked controller are compared, in those cases (47) has a feasible solution. When matrix H is known and the illuminance

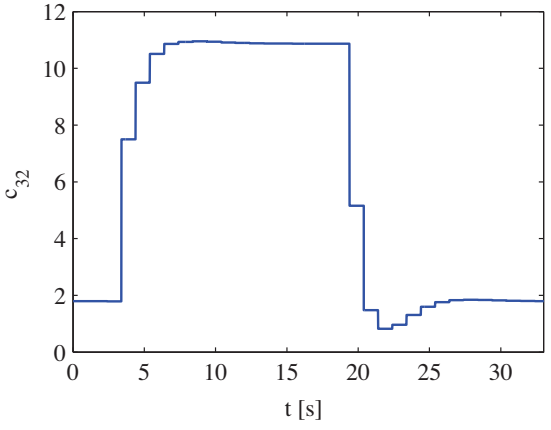

Fig. 12. Message sent to neighbors by controller 32. At $t = 3$, occupancy at zone 15 is detected. At $t = 19$, the zone is unoccupied.

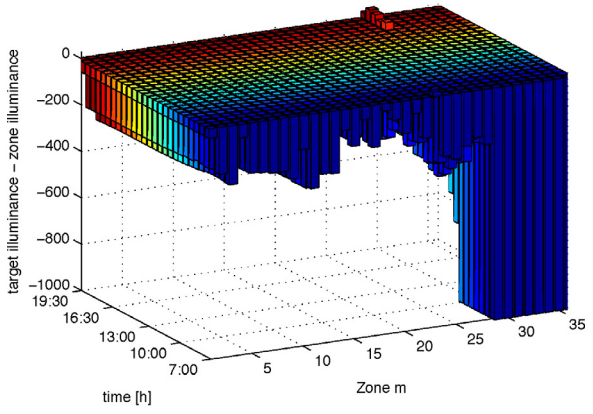

Fig. 14. Steady-state illumination of the zones with daylight from simulation *A*. The positive bars show under-illumination at the zone. The maximum illumination has been capped at 1000 lx for clarity.

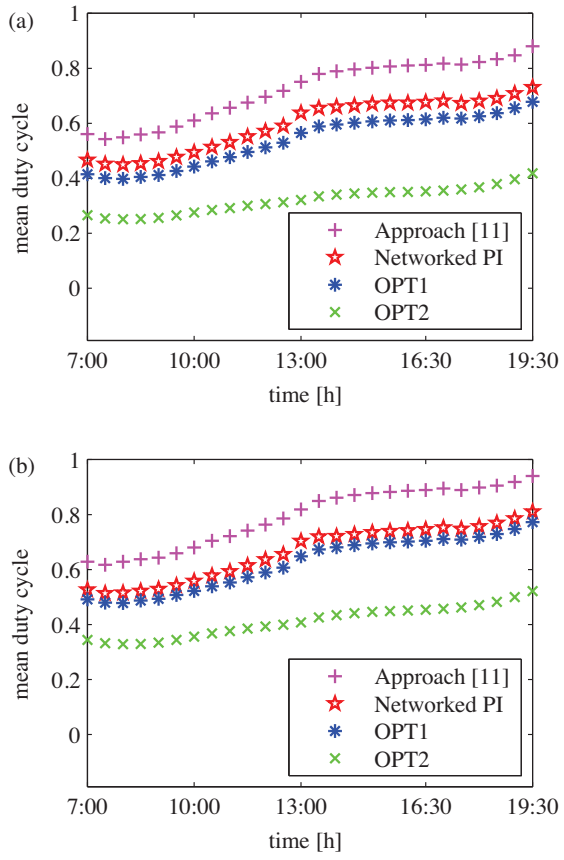

Fig. 15. Mean duty cycle of networked PI controller, OPT1, OPT2 and [11] under simulation *A* with probability of a zone being occupied is (a) 0.3 and (b) 0.6.

values at the workspace plane are known, the following optimization can be directly solved by a centralized controller:

$$\begin{aligned} \text{OPT2}: \min_{\mathbf{u}} \quad & \mathbf{u}\cdot\mathbf{1}^T \quad \text{s.t.} \\ & -H\mathbf{u} \le -\mathbf{W} + \mathbf{p}_s \\ & \mathbf{0} \le \mathbf{u} \le \mathbf{1}, \end{aligned} \tag{48}$$

where $\mathbf{W}$ is the vector with values W_o and W_u and $\mathbf{p}_s$ is the vector of constant daylight at the workspace plane.

To compare the power consumption of the networked PI controller, OPT1 and OPT2, and the one in [11], 10 different static occupancy scenarios where the probability of a zone being occupied is 0.3 and 0.6 are simulated for all 3 full days listed in Table 2, resulting in 1560 simulations for each controller. Fig. 15 shows the mean duty cycle of the four systems for all daylight realizations of simulation *A*, for one occupancy scenario. Because the approach in [11] relies on solving local simplex optimization problems, and uses a weighted average to calculate the duty cycle for the *m*th luminaire, the available power of the *m*th luminaire is not fully exploited to achieve the reference set-point at the *m*th sensor. On the other hand, the networked PI controller exploits the *m*th controller fully to achieve the *m*th reference set-point; therefore the approach in [11] is less power-efficient than the networked PI controller. The difference in average power consumption between the networked PI controller and OPT1 is less than 10% under both occupancy conditions.

8. Conclusions

We presented a distributed lighting control system under two networking scenarios. The controllers sought to meet desired illuminance values at the workspace plane, specified in terms of occupancy-based light sensor set-points that were determined during night-time calibration. Two controller types were considered in stand-alone control. A classical PI controller was used to track a reference, while PI controllers with offset were used to track a reference with a positively biased offset. The considered PI controllers resulted in stable steady-state with an overshoot that was within the required limits for 99.994% of simulation instances. The stand-alone PI controllers were not always capable of reaching the reference set-point, because neighboring controllers are unaware of the under-illumination situation. This was mitigated by adding networking capabilities to the classical PI controller. The power consumption of the networked PI controller was found to be close to that of the centralized controller OPT1 that optimizes duty cycles with light sensor inputs.

References

[1] Energy Information Administration, Commercial Buildings Energy Consumption Survey, 2003.
[2] B. Roisin, M. Bodart, A. Deneyer, P.D. Herdt, Lighting energy savings in offices using different control systems and their real consumption, Energy and Buildings 40 (4) (2008) 514–523.
[3] D. Caicedo, A. Pandharipande, Distributed illumination control with local sensing and actuation in networked lighting systems, IEEE Sensors Journal (2013) 1092–1104.
[4] A. Pandharipande, D. Caicedo, Daylight integrated illumination control of LED systems based on enhanced presence sensing, Energy & Buildings (2011) 944–950.
[5] P.K. Soori, M. Vishwas, Lighting control strategy for energy efficient office lighting system design, Energy & Buildings (2013) 329–337.
[6] EN 12464-1, Light and Lighting – Lighting of Work Places – Part 1: Indoor Work Places, European Committee for Standardization, 2011.
[7] J.H. Lee, Y. Yoon, Y.K. Baik, S. Kim, Analyses on human responses to illuminance variations for resident-friendly lighting environment in a small office, Indoor and Built Environment 22 (3) (2012) 535–550.
[8] F. Rubinstein, G. Ward, R. Verderber, Improving the performance of photoelectrically controlled lighting systems, Journal of the Illuminating Engineering Society (1989).
[9] F. Rubinstein, Photo-electric control of equi-illumination lighting systems, Energy and Buildings 6 (1984) 141–150.
[10] D. Caicedo, A. Pandharipande, G. Leus, Occupancy based illumination control of LED lighting systems, Lighting Research and Technology 38 (4) (2010) 358–376.
[11] H. Wang, A. Pandharipande, D. Caicedo, P.P.J. van den Bosch, Distributed lighting control of locally intelligent luminaire systems, in: IEEE International Conference on Systems, Man and Cybernetics, 2012, pp. 3167–3172.
[12] M.-S. Pan, L.-W. Yeh, Y.-A. Chen, Y.-H. Lin, Y.-C. Tseng, A WSN-based intelligent light control system considering user activities and profiles, IEEE Sensors Journal (2008) 1710–1721.
[13] L.-W. Yeh, C.-Y. Lu, C.-W. Kou, Y.-C. Tseng, C.-W. Yi, Autonomous light control by wireless sensor and actuator networks, IEEE Sensors Journal (2010) 1029–1041.
[14] Y-J. Wen, A.M. Agogino, Personalized dynamic design of networked lighting for energy-efficiency in open-plan offices, Energy & Buildings 43 (8) (2011) 1919–1924.
[15] M. Miki, A. Amamiya, T. Hiroyasu, Distributed optimal control of lighting based on stochastic hill climbing method with variable neighborhood, in: IEEE International Conference on Systems, Man and Cybernetics, 2007, pp. 1676–1680.
[16] G.F. Franklin, M.L. Workman, D. Powell, Digital Control of Dynamic Systems, Addison-Wesley Publishing Co. Inc., 1990.
[17] S. Tarbouriech, G. Garcia, J.M.G. da Silva, I. Queinnec, Stability and Stabilization of Linear Systems with Saturating Actuators, Springer-Verlag, 2011.
[18] Philips BBS560 product leaflet, Online: http://download.p4c.philips.com/l4b/9/910502003703_eu/910502003703_eu_pss_aenaa.pdf
[19] DIAL Gmbh, DIALux 4.11, Online: http://www.dial.de/DIAL/en/dialux/download.html